Influence of illumination spectrum on dissociation kinetic of iron-boron pairs in silicon

Oleg Olikh Oleksandr Datsenko Serhiy Kondratenko*

Prof. O. Olikh, Dr. O. Datsenko, Prof. S. Kondratenko
Taras Shevchenko National University of Kyiv, 64/13, Volodymyrska Street, 01601, Kyiv, Ukraine
Email Address: olegolikh@knu.ua

Keywords: *silicon, iron-boron pairs, light-induced dissociation, light source impact*

Please insert your abstract here

1 Introduction

Defects significantly impact semiconductor properties. Although minimizing device dimensions to nanometers shifts some focus from extensive to point defects, physical properties still rely heavily on the presence and distribution of these irregularities. Hence, many strategies for enhancing semiconductor structures, including radiation and temperature treatments or certain fabrication conditions, strive to decrease the defect concentration or neutralize its effects [1, 2, 3]. For instance, in the case of photovoltaic devices, we must understand and optimize the carrier properties tied to defects and impurities [1]. Such controlled alteration methods of the defective subsystem have been generalized under the term "defect engineering" and are extremely important from a practical standpoint.
Successful defect engineering hinges on an in-depth understanding of defect properties. Key factors are defect formation energy, transition energy levels, self-compensating effects, nonradiative recombination caused by defects, and the mechanism of reconstruction and diffusion [1]. Considering the extraordinary diversity of possible intrinsic and impurity defects, complete information on all of them is lacking even for silicon, which is the most studied semiconductor. Nevertheless, it must be noted that considerable data have been amassed on silicon, and have a solid understanding of some defects [4].
For instance, such defects are iron impurity, a common, detrimental, and often unavoidable contaminant in photovoltaic silicon [3, 5], and iron-boron pair. Specifically, iron atoms are known to be at the interstitial sites, and Fe_i^+ are highly efficient recombination centers [6]. In p-type Si at room temperature, iron atoms are almost predominantly bound in complexes with dopants (B, Ga, Al, In). This defect demonstrates bistable behavior: the stable state is defined by the configuration in which the Fe occupies the first nearest tetrahedral interstitial site closest to the substituent atom, whereas, in the metastable configuration, Fe is at the second T_d interstitial site [7]. The energy levels associated with iron and its complexes, as well as the respective carriers capture cross-sections, are well-established [4, 8]. Among the acceptor-iron pairs, the complex FeB is the most thoroughly investigated, primarily due to the widespread use of Si:B in the fabrication of various devices, such as solar cells. However, it is worth mentioning that gallium is gaining increasing attention as an acceptor dopant whose incorporation, for instance, can help mitigate the light and elevated temperature-induced degradation [9].
The dynamics of FeB pairs are also examined. It's established that FeB pairs can be dissociated through illumination, minority carrier injection, and thermal treatment at 200 °C [10]. In the context of illumination, the dissociation rate R_d is influenced by the overall carrier generation rate G [11, 10, 12, 13]:

$$R_d = K\left(\frac{G}{N_{\mathrm{FeB}}}\right)^2, \tag{1}$$

where N_{FeB} is the pair concentration, K is the constant of material. To achieve almost complete dissociation of the FeB pair, it is necessary for the illumination power to exceed 0.1 W cm^{-2} [14]. The dissociation process of FeB pairs by electron capture unfolds in two stages [15, 10]: the initial stage involves

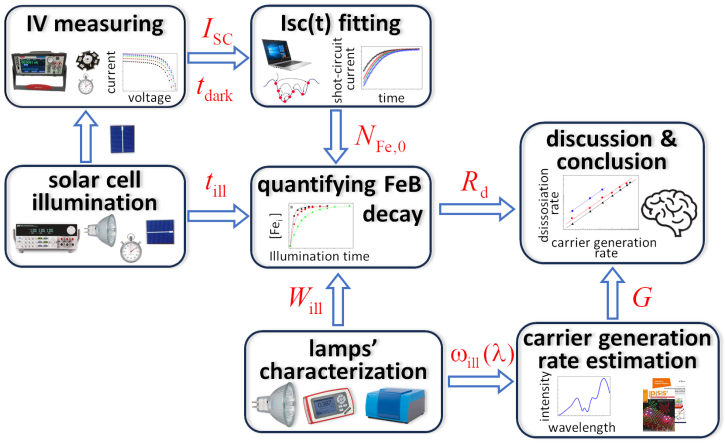

Figure 1: Investigation framework

the neutralization of Fe and the elimination of the Coulombic attraction between the pair components. The mechanism of the second stage is contentious; it may involve either the recharge of the iron ion or the recombination-enhanced defect reaction (REDR) triggered by electron-hole recombination.

It should be noted that despite the extensive data on the properties of iron-related defects in silicon, intensive research persists. In particular, efforts focus on analyzing the impact of high-intensive illumination [16] or dopant compensation [17], alongside clarifying the second-stage mechanism of dissociation [5] or reassessing recombination parameters [18].

This study aims to investigate the effect of the light spectrum on the dissociation kinetics of FeB pairs in silicon. While pair dissociation is typically carried out using a halogen lamp [11, 5] or 904 nm laser [16, 10, 19], there is limited understanding of how the light source influences this process. By studying the impact of different illumination spectra on FeB dissociation, we aim to provide valuable insights for defect engineering and the efficient transformation of detrimental impurity iron atoms into a highly mobile interstitial state within the active region of a silicon device. Besides, such information, in our opinion, can help make the right choice between existing options for the second stage of pair decay.

Figure 1 illustrates the main stages of the research. Initially, the dissociation rate of FeB pairs under illumination of the solar cell with different integral intensities was determined. For this purpose, the dependence of the quantity of interstitial iron atoms formed over time under intense illumination was measured. The concentrations of formed pairs were measured by investigating the kinetics of short-circuit current. Three light sources from different manufacturers were used (further details are described in Section 1). To determine the carrier generation rate, spectra of sample illumination using various light sources were measured, taking into account the effects of light reflection, absorption by free carriers, and effective absorption depths. The obtained results led to the conclusion that the efficiency of light-induced dissociation increases with decreasing photon wavelength.

In Figure 1, the main stages of the research are illustrated. First step was determination of the dissociation rate of FeB pairs under illumination with different integral intensities. Three light sources from different manufacturers were used (further details are described in Section 4). To measure number of interstitial iron atoms formed over fixed time under strong illumination the kinetics of short-circuit current was used. The result is presented in Section 2.1. Section 2.2 deals with estimating the carrier generation rate using spectra of sample illumination and considering the effects of light reflection, absorption by free carriers, and effective absorption depths. The obtained results showed that the efficiency of light-induced dissociation increases with decreasing photon wavelength — see Section 2.3. Finally, we conclude this paper in Section 3.

2 Results and Discussion

2.1 Dissociation rate determination

The equilibrium between free Fe_i and Fe_iB_s is known to be determined by the following equations [20, 5, 10]

$$Fe_i + B_s \underset{R_d}{\overset{R_a}{\rightleftharpoons}} FeB\,, \tag{2}$$

where R_a is the association rate. As a result, the concentration of interstitial iron atoms N_{Fe_i} depending on illumination time t_{ill} during light-induced dissociation can be described as follows [11, 12, 21]

$$N_{Fe_i}(t_{ill}) = \left(N_{Fe,eq} - N_{Fe,tot}\frac{R_d}{R_d+R_a}\right)\exp[-(R_d+R_a)t_{ill}] + N_{Fe,tot}\frac{R_d}{R_d+R_a}\,, \tag{3}$$

where $N_{Fe,tot}$ is the total concentration of the impurity iron, $N_{Fe,eq}$ represents the concentration of unpaired interstitial iron atoms in the equilibrium state (in darkness, $N_{Fe,eq} = N_{Fe_i}(t_{ill} = 0)$). It's important to highlight that $N_{Fe,eq}$ is significantly influenced by temperature and the Fermi level location [20]. Specifically, in the case of p-type Si with a hole concentration of 1.36×10^{15} cm^{-3} (which corresponds to the base of the structure under investigation), at a temperature of $T = 300$ K, $N_{Fe,eq}$ constitutes merely about 1% of $N_{Fe,tot}$, rendering it negligible for practical considerations. However, when the temperature rises to 340 K, the proportion of $N_{Fe,eq}$ increases to approximately 14.5%.

After the cessation of illumination, only the process of association occurs, and the time dependence of Fe_i concentration can be expressed as follows [20, 22]:

$$N_{Fe_i}(t_{dark}) = (N_{Fe,0} - N_{Fe,eq}) \times \exp(-R_a t_{dark}) + N_{Fe,eq}\,, \tag{4}$$

where t_{dark} is the time after strong illumination stopping, $N_{Fe,0}$ is the concentration of interstitial iron atoms formed after illumination, $N_{Fe,0} = N_{Fe_i}(t_{dark} = 0) = N_{Fe_i}(t_{ill})$.

The study examined the dependence of $N_{Fe,0}$ in silicon solar cells on illumination time t_{ill} using different illumination intensities W_{ill} (200 − 750 mW) and light sources (three halogen lamps, labeled as Orion, Osram, and GE, and described in detail in Section 4). The experiments were conducted at a temperature of 340 K. The values of $N_{Fe,0}$ were determined using a methodology [23, 21] based on the study of the kinetics of short-circuit current I_{SC} under low-intensity monochromatic illumination. Specifically, after strong illumination with a duration of t_{ill}, the current-voltage characteristic (IV) of the solar cell was measured every 21 seconds over a time t_{dark} interval of approximately 3000 seconds.

Figure 2a shows some typical IV curves. It can be seen that upon cessation of illumination, there exists a gradual augmentation in both the short-circuit current and the open-circuit voltage. This phenomenon is indicative of a decrease in the recombination activity of the defective subsystem, which is a result of the transition of interstitial iron to a bound state with an acceptor. Moreover, at the end of the measurement interval, the minute changes in the IV curves denote that the selected interval of 50 minutes is sufficient to complete the association.

Figure 2b illustrates the dependencies $I_{SC}(t_{dark})$ after illumination with different intensities. As previously shown [21], the magnitude of the change in I_{SC} after the dark recovery period inherently correlates with the concentration of Fe_i formed as a result of light-induced dissociation of FeB pairs. From examining the presented data, it is evident that escalating W_{ill} leads to an augmentation in the dissociation efficiency. Concurrently, the recovery time remains insensitive to the illumination parameters, which conforms to expectations, given that the latter is determined by R_a — see Equation (4).

It should be noted that besides $N_{Fe,0}$ values, the methodology used allows for the estimation of the energy of Fe_i migration E_m and bulk lifetime τ_{other}, which arises from recombination channels other than Fe-related defects and intrinsic recombination. The obtained value $E_m = (0.650 \pm 0.005)$ eV coincides with that wellknown value [12, 24, 25]. This coincidence confirms that the investigated processes are indeed associated with rebuilding, as described by Equation (2). The value of E_m allows for the estimation

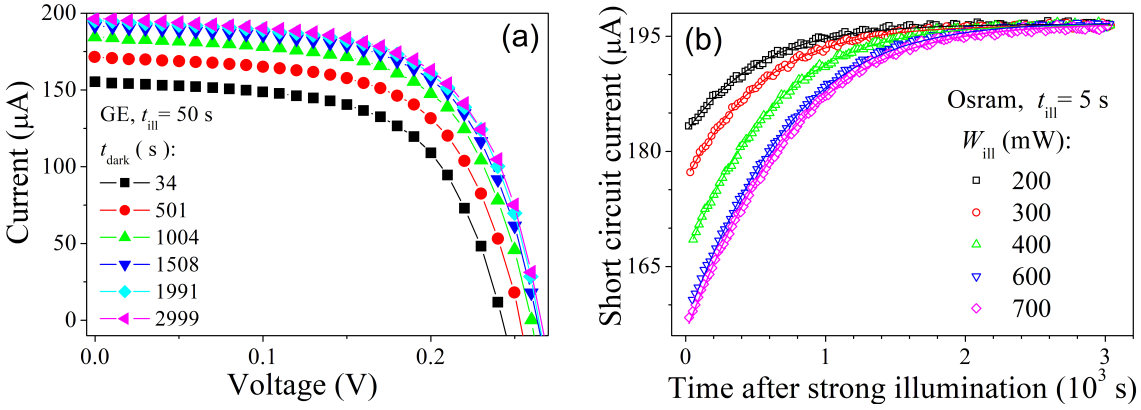

Figure 2: Typical current-voltage characteristics measured under low-intensive (LED) illumination across different periods following exposure to strong light (halogen lamp) (panel a) and short circuit current plotted as a function of the time after high-intensive illumination (panel b). The marks are the experimental results and the lines on panel b are the curves fitted according to [23, 21]. Light sources: GE (a), Osram (b). t_{ill}, s: 50 (a), 5(b). $W_{ill} = 400$ mW (a). $T = 340$ K.

of the recombination rate [10, 12, 24]:

$$R_a^{-1} = 5.7 \times 10^5 \frac{\text{s}}{\text{K cm}^3} \times \frac{T}{p} \exp\left(\frac{E_m}{kT}\right) . \tag{5}$$

Thus, in our case, $R_a = (1.68 \pm 0.03) \times 10^{-3}$ s^{-1}.
Regarding the value of τ_{other}, it was found to significantly exceed the lifetime associated with Shockley-Read–Hall (SRH) recombination on Fe-related defects. Notably, according Möller *et al.* [10], such a condition is essential for the accurate determination of the constant K, which is included in Equation (1).
The dependencies of the concentration of interstitial atoms on illumination time are shown in Figure 3. From the data, it's evident that the pair dissociation rate is significantly influenced by the illumination intensity. This effect is consistent across all utilized light sources. Nonetheless, the W_{ill} value is not the exclusive determining factor for the pair dissociation rate, as demonstrated in Figure 3d. For instance, when using the GE source, pair dissociation occurs most efficiently. With Osram, the process unfolds more slowly, and illumination with Orion, under otherwise identical conditions, proves to be the least effective in terms of altering the state of FeB pairs.
The $N_{Fe,0}(t_{ill})$ dependencies were fitted using the equation

$$N_{Fe,0}(t_{ill}) = A \exp(-t_{ill}/\tau_{dis}) + N_{Fe,fit} , \tag{6}$$

where τ_{dis} is the characteristic dissociation time, and $N_{Fe,fit}$ concentration of dissociated pairs at saturation. The fitting results, shown in Figure 3 as lines and listed in the Table 1, include the coefficients of determination R^2. The high values of R^2 (greater than 0.99) confirm the suitability of the chosen approximation formula.
The comparison of Equations (3) and (6) reveals a relationship between the fitting parameters and defect characteristics, specifically:

$$\tau_{dis}^{-1} = R_a + R_d , \tag{7}$$

$$N_{Fe,fit} = N_{Fe,tot} \frac{R_d}{R_d + R_a} . \tag{8}$$

Table 1 suggests that regardless of the light source used and W_{ill}, the observed total concentration of impurity iron atom is consistently $N_{Fe,tot} = (8.7 \pm 0.1) \times 10^{12}$ cm^{-3}. This stability supports the accuracy of the analysis. However, the FeB dissociation rate may vary significantly for the same intensity value depending on the light source used.
According to Wijaranakula [20], at the specified value of $N_{Fe,tot}$, the equilibrium (in darkness) concentrations of interstitial iron atoms $N_{Fe,eq}$ and FeB pairs N_{FeB} at $T = 340$ K are 1.3×10^{12} cm^{-3} and

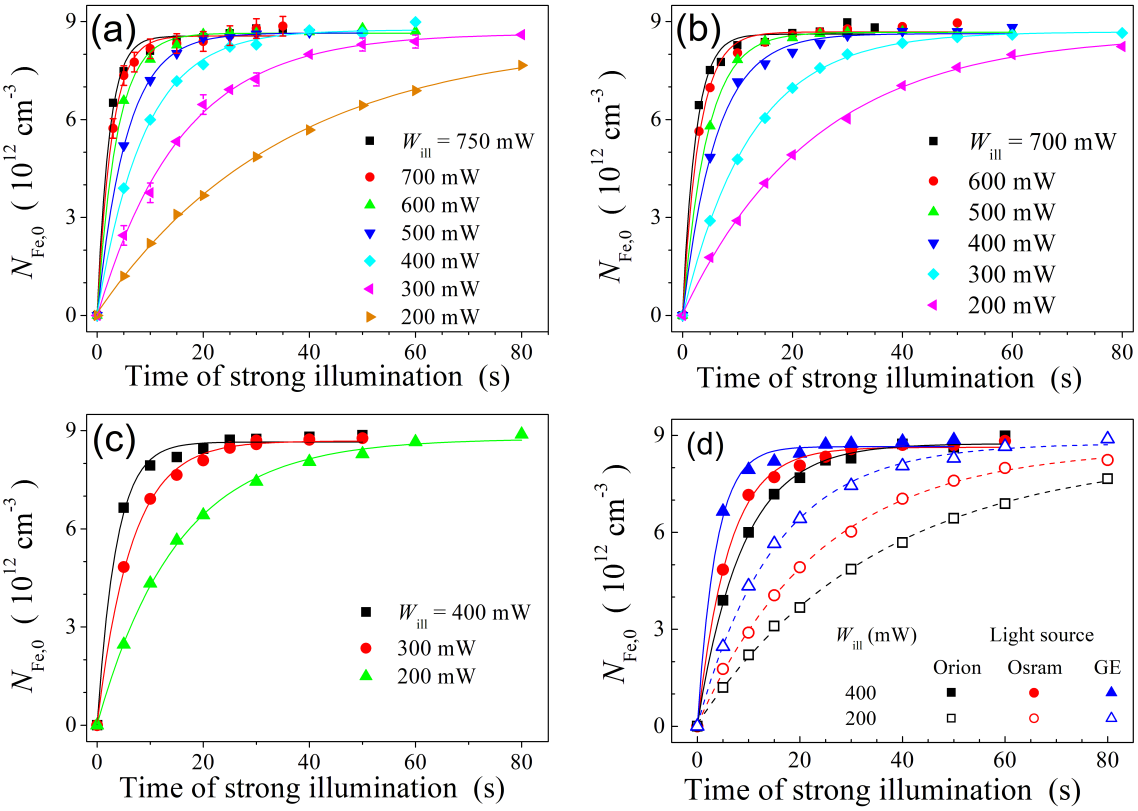

Figure 3: The relationships between the concentration of FeB pairs following intense illuminations of varying intensities and the illumination duration. Light source: Orion (a), Osram (b), GE (c). Panel d highlights variations in the dissociation of pairs induced by different light sources. The marks are the experimental results, the lines are the fitted curves using Equation (6). $T = 340$ K.

Table 1: Fitting results of experimental dependencies $N_{Fe,0}(t_{ill})$ using Equation (6) and defect parameter estimation using Equations (7-8).

W_{ill} [mW]	Light source	fitting parameters			defect parameters	
		τ_{dis} [s]	$N_{Fe,fit}$ [10^{12} cm^3]	R^2	R_d [10^{-3} s^{-1}]	$N_{Fe,tot}$ [10^{12} cm^{-3}]
750	Orion	2.2 ± 0.2	8.6 ± 0.1	0.993	450	8.6
700	Orion	2.7 ± 0.2	8.7 ± 0.1	0.995	370	8.7
	Osram	2.4 ± 0.2	8.6 ± 0.1	0.992	410	8.6
600	Orion	3.7 ± 0.2	8.65 ± 0.06	0.998	270	8.7
	Osram	3.0 ± 0.2	8.69 ± 0.08	0.995	330	8.7
500	Orion	5.5 ± 0.2	8.65 ± 0.04	0.999	180	8.7
	Osram	4.5 ± 0.1	8.7 ± 0.1	0.998	220	8.8
400	Orion	8.8 ± 0.3	8.74 ± 0.06	0.998	110	8.8
	Osram	6.1 ± 0.2	8.63 ± 0.08	0.997	160	8.7
	GE	3.6 ± 0.3	8.7 ± 0.1	0.996	280	8.7
300	Orion	15.7 ± 0.6	8.6 ± 0.1	0.998	62	8.8
	Osram	12.4 ± 0.1	8.69 ± 0.02	0.999	79	8.8
	GE	6.5 ± 0.2	8.69 ± 0.05	0.998	150	8.8
200	Orion	35 ± 3	8.5 ± 0.3	0.998	27	8.8
	Osram	24 ± 1	8.6 ± 0.1	0.999	40	8.9
	GE	15.1 ± 0.5	8.7 ± 0.1	0.999	65	8.8

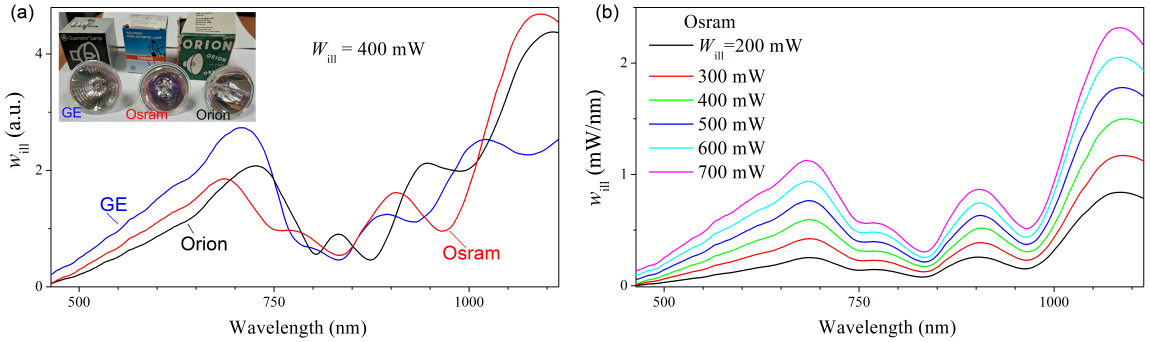

Figure 4: The spectra of sample illumination in the case of using different light sources with the same integral intensity W_{ill} = 400 mW (panel a) and a single source (Osram) at various W_{ill} values (panel b). The inset shows photos of light sources.

7.4×10^{12} cm^{-3}, respectively. The values of $N_{\mathrm{Fe,eq}}$ and N_{FeB} were used to estimate the minority carrier diffusion length L_n in the base of the used solar cell. It was assumed that the dominant recombination processes are SRH recombination at Fe_i and FeB and intrinsic recombination. The required electron mobility μ_n value were taken from Klaassen [26], the capture cross sections and energy levels for Fe_i and FeB from Rougieux *et al.* [8], the coefficients of band-to-band radiation recombination and Auger recombination from Niewelt *et al.* [27] and Black & Macdonald [28], respectively. The calculated value was found to be L_n = 80 μm, which is remarkably close to the value of 86 μm obtained from the study of temperature dependencies of short-circuit current — see Supplementary materials.

2.2 Carrier generation rate estimation

The dissociation rate of FeB pairs during light-induced decay is well known to be dependent on the carrier generation rate — see Equation (1). Our subsequent objective involved determining the values of G for various light sources. The measured dependencies of spectral intensity w_{ill} of illumination incident on the sample under diverse conditions, are shown in Figure 4. It is crucial to highlight that our focus is specifically on the light reaching the sample; hence, the spectrum is altered not only by the infrared transparency of the lamp reflector but also by absorption in the fiber utilized to transmit the light flux to the solar cell. Analogous modifications to the illumination spectra have been observed previously [29]. Figure 4a displays discrepancies in the illumination spectra obtained from different light sources, attributed to variations in the operational temperatures of the halogen lamps and differences in reflectors (photos of the lamps are in the inset of Figure 4a). It is important to note that the upper limit of the spectra in Fig 4 is limited by the silicon bandgap, which, according to Passler [30], corresponds to 1.11 eV at 340 K. Furthermore, Figure 4b demonstrates the change in the Osram spectrum with integral intensity increasing. Notably, in addition to the expected increase in the curve's area, a minor spectrum shift towards shorter wavelengths is observed. These behaviour is typical for all used light sources. Carrier generation rate was estimated as follows:

$$G = \int g(\lambda) d\lambda \,, \tag{9}$$

where spectral carrier generation rate g

$$g = \frac{w_{\mathrm{ill}}\lambda}{hc} \frac{(1-R)A_{\mathrm{bb}}}{S\, d_{\mathrm{eff}}} \,, \tag{10}$$

where $n_{\mathrm{ph}} = \frac{w_{\mathrm{ill}}\lambda}{hc}$ is the spectral photon flux, R is the is the coefficient of reflection, A_{bb} is the fraction of the band-to-band transitions, S is illuminated square of sample, d_{eff} is the effective width of carrier generation.

In calculating the value of R, we employed an approach [31], which accounted for the presence of antireflective and passivating layers on the front surface of the sample, as well as the effects of multiple reflections. The resulting spectral dependence of R is shown in Figure S3 of the Supplementary materials.

The expression for the e-h pair generating fraction of the Lambertian absorptance in a solar cell can be written as [32]:

$$A_{\rm bb}(\lambda) = \frac{\alpha_{\rm bb}}{\alpha_{\rm bb}+\alpha_{\rm fca}} \frac{(1-T_r)(1+T_r)n_r^2}{n_r^2-(n_r^2-1)T_r^2}\,, \tag{11}$$

with

$$\begin{aligned} T_r &= (1-x)\exp(-x) + x^2 E_1(x)\,, \\ x &= (\alpha_{\rm bb}+\alpha_{\rm fca})d\,, \\ E_1(x) &= \int_x^\infty t^{-1}\exp(-t)dt\,, \end{aligned}$$

where $\alpha_{\rm bb}$ is the absorption coefficient due to e–h pair generation by band-to-band transitions; $\alpha_{\rm fca}$ is the absorption coefficient due to free carrier absorption; n_r is the refractive index; d is the width of the device.

In our calculations of $A_{\rm bb}$ by using Equations (11), we took $\alpha_{\rm bb}$ and n_r from Green[33], $\alpha_{\rm fca}$ from Baker-Finch *et al.* [34]. The spectral dependence of the fraction of the band-to-band transitions can be found in Supplementary materials (Figure S5).

When determining the carrier generation volume, we applied Bowden&Sinton approach [35] to thick silicon wafers, where the diffusion length or light absorption depth is significantly less than the sample thickness. In these cases, the distribution of carriers is heavily skewed toward the illuminated surface, rendering the use of the arithmetic mean of carrier concentration unsuitable. Consequently, the average values are computed using carrier concentration as a weighting function, and effective generation region width is determined as follows [35]:

$$d_{\rm eff}(\lambda) = \frac{\left(\int_0^d \Delta n dx\right)^2}{\int_0^d \Delta n^2 dx}\,, \tag{12}$$

where Δn is the increase in minority carrier density due to illumination

$$\Delta n(x) = \frac{\alpha_{\rm bb} n_{\rm ph} L_n^2 q}{(\alpha_{\rm bb}^2 L_n^2 - 1)kT\mu_n}\left[\exp\left(-\frac{x}{L_n}\right) - \exp\left(-\alpha_{\rm bb}x\right)\right]\,. \tag{13}$$

In calculations, we used L_n value, determined in Section 2.1. Some dependencies for different L_n values are shown in Figure S4 (Supplementary materials).

The consideration of dependencies $R(\lambda)$, $A_{\rm bb}(\lambda)$, and $d_{\rm eff}(\lambda)$ alters the spectral carrier generation rate compared to the spectral photon flux, leading to an increased contribution to e-h pairs generating from shorter wavelength light, as illustrated in Figure 5a. In Figure 5b, variations in the total carrier generation rate are depicted with increasing light intensity for different light sources. It is evident that differences exist between the light sources, yet the absolute contrasts in the magnitude of G for various light sources under $W_{\rm ill} = const$ conditions do not surpass 2 percent, with Orion registering the highest carrier generation rate value. Notably, without considering R, $A_{\rm bb}$, and $d_{\rm eff}$ and calculating G as the ratio of incident photons number to the total sample volume, the qualitative outcomes would remain quite similar. The main difference would lie in the absolute values of the carrier generation rate.

Thus, the discrepancies previously (Section 2.1) noticed in the value of R_d under identical illumination intensity levels cannot be attributed to variations in the carrier generation rate among different light sources, even when factoring in the quadratic dependency of the dissociation rate on G. Hence, there must be another underlying cause for these differences.

2.3 Effect of illumination spectrum on FeB pair decay

The dependencies $R_d(G)$ in logarithmic scale are presented in Figure 6a. The linear patterns observed in the data indicate a clear power law relationship between the dissociation rates of FeB pairs and the

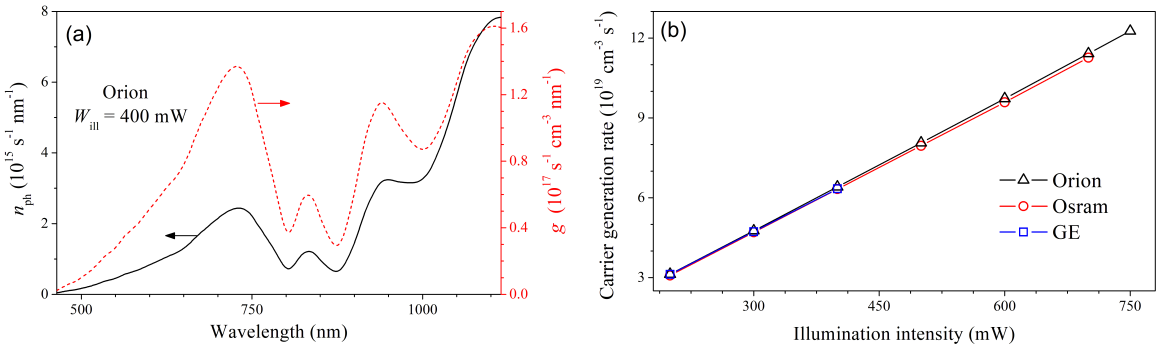

Figure 5: (a) Photon flux spectral density (left axis, solid line) and carrier generate rate spectral density (right axis, dashed line). Orion light source, $W_{\text{ill}} = 400$ mW. (b) Dependencies of carrier generation rate on illumination intensity for different light sources.

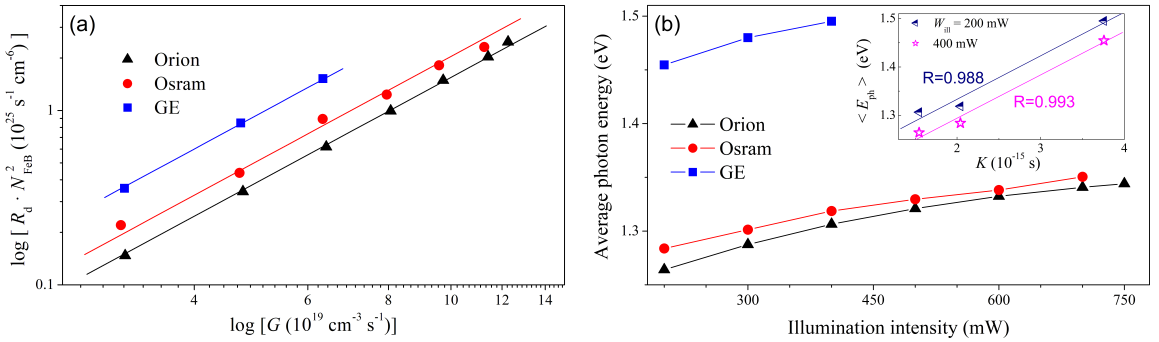

Figure 6: (a) FeB pair dissociation rate plotted as $R_d \cdot N_{\text{FeB}}^2$ over the light induced generation rate. The solid lines show the quadratic dependence according to Equation (1). (b) Dependencies of average photon energy on illumination intensity for different light sources. The inset shows prefactor K vs average photon energy for the different light sources and illumination intensities. The lines are linear fitted curves. Coefficients of correlation are shown as well.

carrier generation rate. The figure also exhibits the fit results using Equation (1). High correlation coefficients exceeding 0.998 validate the applicability of the quadratic dependence expressed by Equation (1) to our data. It should be noted that Khelifati *et al.* [12] stipulate the inclusion of $Rd\,(1+\tau_{\text{FeB}}/\tau_{\text{other}})^2$ (where τ_{FeB} is the lifetime associated with recombination on FeB pairs) on the left-hand side of Equation (1) rather than R_d. However, in our cases $\tau_{\text{other}} \gg \tau_{\text{FeB}}$, as previously acknowledged in Section 2.1, this additional multiplier can be disregarded.

The prefactor K values determined from the fitting are 3.8×10^{-15} s for the GE light source, 2.0×10^{-15} s for the Osram, and 1.5×10^{-15} s for the Orion source. K serves as a important parameter linked to the phenomenon of FeB pairs' dissociation by illumination [12], and the values obtained in this study are compared with those ($4.2\times10^{-17} - 5\times10^{-15}$ s) previously presented [11, 10, 12]. It is essential to note that in prior research, disparities in the constant K value for diverse samples were ascribed to variations in defect composition and the presence of alternative recombination channels apart from iron-related defects [11, 10]. However, in our case, distinct K values were obtained for the same structure under identical conditions, such as temperature and integrated light intensity, with differences in the illumination spectra only.

In other words, the obtained data indicate that in the analysis of light-induced dissociation of FeB pairs, it is necessary to consider not only the quantity of photo-generated excess charge carriers but also the energies of the photons that lead to their appearance. For such an energy characterization of light sources, we used the average photon energy $< E_{\text{ph}} >$:

$$< E_{\text{ph}} >= \frac{\int \frac{hc}{\lambda} n_{\text{ph}}(\lambda) d\lambda}{\int n_{\text{ph}}(\lambda) d\lambda}\,. \tag{14}$$

The summary of the results concerning the $< E_{\text{ph}} >$ values is shown in Figure 6b. In particular, it demon-

strates the shift of the emission spectrum of light sources towards the short-wavelength region with an increase in the W_{ill} value, as illustrated in Figure 4a. And a clear conclusion can be drawn upon comparing the data in Figures 3,5b, 6a, 6b and Table 1: with rising average photon energy, the light-induced dissociation of FeB pairs becomes more pronounced. Specifically, the constant K increases, the dissociation rate R_d escalates, and correspondingly, the illumination time necessary for a complete complex decay decreases. Consequently, for the dissociation of FeB pairs, the energy expended during the thermalization of non-equilibrium carriers also holds significance.
The obtained results offer some conclusions about the mechanism of FeB dissociation. As discussed in the literature and previously mentioned, two possible ways of the second decay stage are typically considered: REDR and the recharge of the iron ion. REDR arises from strong electron-lattice coupling at the defect site and involves the utilization of local vibrational energy to promote pair dissociation [10, 5, 14]. The observed correlation between dissociation rate and photon energy in this study supports the REDR process. Specifically, as photon energy increases, the production of non-equilibrium phonons during thermalization also rises. Furthermore, the increase in R_d value, as found in the experiment, signifies the active involvement of these quasi-particles in the dissociation of FeB pairs. Notably, recent research [5] focusing on a detailed analysis of the dissociation and association reactions of the iron-boron pairs similarly concluded the predominant role of REDR processes.

3 Conclusion

4 Experimental Section

The n^+-p-p^+-Si samples were used in the experiment. The structure was fabricated from a 380 μm thick p-type boron-doped Czochralski silicon wafer with [100] orientation and hole concentration $p = 1.36 \times 10^{15}$ cm^{-3}. The n^+ emitter with sheet resistance of about $20 - 30$ $\Omega/\square$ and thickness of 0.7 μm was formed by phosphorus diffusion. The anti-recombination isotype barrier was created by using p^+ layer ($10 - 20$ $\Omega/\square$, 0.6 μm) formed by boron diffusion. On the front surface, the antireflective and passivating SiO_2 (40 nm) and Si_3N_4 (30 nm) layers were formed. The solid and grid Al contacts were formed by magnetron sputtering on the rear and front surfaces respectively.
Three powerful halogen lamps from different manufacturers were employed for the light-induced dissociation of FeB pairs:

- Orion Haltlichtspiegel 52240.0, 24 V, 200 W (labeled Orion in the paper);
- Osram 64653 HLX ELC, 24 V, 250 W (Osram);
- General Electric 43537 H271, 20 V, 150 W (GE);

The temperature was maintained constant using a PID (proportional-integral-derivative controller) algorithm which is implemented in the software which serves the system.
Therefore, the temperature of the wafers was regulated and controlled through a thermoelectric cooling system based on the Peltier effect

First part of experimental section:

Second part of experimental section:

Supporting Information
Supporting Information is available from the Wiley Online Library or from the author.

Acknowledgements
The authors are grateful for the help with calculating the coefficient of reflection by solar cells to Prof. Vitaliy Kostylyov.

Conflict of Interest The authors declare no conflict of interest.

References

[1] X. Cai, S.-H. Wei, *J. Appl. Phys.* **2023**, *134*, 22 220901.

[2] J. Vobecky, *Phys. Status Solidi A* **2021**, *218*, 23 2100169.

[3] J. Frascaroli, P. Monge Roffarello, I. Mica, *Phys. Status Solidi A* **2021**, *218*, 23 2100206.

[4] M. K. Juhl, F. D. Heinz, G. Coletti, D. Macdonald, F. E. Rougieux, F. Schindle, T. Niewelt, M. C. Schubert, In *2018 IEEE 7th World Conference on Photovoltaic Energy Conversion (WCPEC) (A Joint Conference of 45th IEEE PVSC, 28th PVSEC & 34th EU PVSEC)*. **2018** 0328–0332.

[5] C. Sun, Y. Zhu, M. Juhl, W. Yang, F. Rougieux, Z. Hameiri, D. Macdonald, *Phys. Status Solidi RRL* **2021**, *15*, 12 2000520.

[6] E. Weber, *Appl. Phys. A* **1983**, *30*, 1 1.

[7] H. Nakashima, T. Sadoh, T. Tsurushima, *Phys. Rev. B* **1994**, *49*, 24 16983.

[8] F. E. Rougieux, C. Sun, D. Macdonald, *Sol. Energy Mater. Sol. Cells* **2018**, *187* 263 .

[9] L. Ning, L. Song, J. Zhang, *J. Alloys Compd.* **2022**, *912* 165120.

[10] C. Möller, T. Bartel, F. Gibaja, K. Lauer, *J. Appl. Phys.* **2014**, *116*, 2 024503.

[11] L. J. Geerligs, D. Macdonald, *Appl. Phys. Lett.* **2004**, *85*, 22 5227.

[12] N. Khelifati, H. S. Laine, V. Vähänissi, H. Savin, F. Z. Bouamama, D. Bouhafs, *Phys Status Solidi A* **2019**, *216*, 17 1900253.

[13] S. Herlufsen, D. Macdonald, K. Bothe, J. Schmidt, *physica status solidi (RRL) – Rapid Research Letters* **2012**, *6*, 1 1.

[14] D. H. Macdonald, L. J. Geerligs, A. Azzizi, *J. Appl. Phys.* **2004**, *95*, 3 1021.

[15] L. Kimerling, J. Benton, *Physica B+C* **1983**, *116*, 1 297.

[16] X. Zhu, D. Yang, X. Yu, J. He, Y. Wu, J. Vanhellemont, D. Que, *AIP Adv.* **2013**, *3*, 8 082124.

[17] X. Zhu, X. Yu, P. Chen, Y. Liu, J. Vanhellemont, D. Yang, *Int. J. Photoenergy* **2015**, *2015* 154574.

[18] T. T. Le, Z. Zhou, A. Chen, Z. Yang, F. Rougieux, D. Macdonald, A. Liu, *J. Appl. Phys.* **2024**, *135*, 13 133107.

[19] K. Lauer, C. Möller, D. Debbih, M. Auge, D. Schulze, In *Gettering and Defect Engineering in Semiconductor Technology XVI*, volume 242 of *Solid State Phenomena*. Trans Tech Publications Ltd, **2016** 230–235.

[20] W. Wijaranakula, *J. Electrochem. Soc.* **1993**, *140*, 1 275.

[21] O. Olikh, V. Kostylyov, V. Vlasiuk, R. Korkishko, Y. Olikh, R. Chupryna, *J. Appl. Phys.* **2021**, *130*, 23 235703.

[22] J. D. Murphy, K. Bothe, M. Olmo, V. V. Voronkov, R. J. Falster, *J. Appl. Phys.* **2011**, *110*, 5 053713.

[23] O. Olikh, V. Kostylyov, V. Vlasiuk, R. Korkishko, R. Chupryna, *J. Mater. Sci.: Mater. Electron.* **2022**, *33*, 16 13133.

[24] J. Tan, D. Macdonald, F. Rougieux, A. Cuevas, *Semicond Sci. Technol.* **2011**, *26*, 5 055019.

[25] D. Macdonald, A. Cuevas, L. J. Geerligs, *Appl. Phys. Lett.* **2008**, *92*, 20 202119.

[26] D. Klaassen, *Solid-State Electron.* **1992**, *35*, 7 953.

[27] T. Niewelt, B. Steinhauser, A. Richter, B. Veith-Wolf, A. Fell, B. Hammann, N. Grant, L. Black, J. Tan, A. Youssef, J. Murphy, J. Schmidt, M. Schubert, S. Glunz, *Sol. Energ. Mat. Sol.* **2022**, *235* 111467.

[28] L. E. Black, D. H. Macdonald, *Sol. Energ. Mat. Sol.* **2022**, *234* 111428.

[29] M. Libra, V. Poulek, P. Kourim, *Research in Agricultural Engineering* **2017**, *63*, 1 10.

[30] R. Pässler, *Phys. Rev. B* **2002**, *66* 085201.

[31] N. Klyui, V. Kostylyov, A. Rozhin, V. Gorbulik, V. Litovchenko, M. Voronkin, N. Zaika, *Opto-Electr. Rev.* **2000**, *8*, 4 402.

[32] S. Schäfer, R. Brendel, *IEEE J. Photovolt.* **2018**, *8*, 4 1156.

[33] M. A. Green, *Prog. Photovoltaics Res. Appl.* **2022**, *30*, 2 164.

[34] S. C. Baker-Finch, K. R. McIntosh, D. Yan, K. C. Fong, T. C. Kho, *J. Appl. Phys.* **2014**, *116*, 6 063106.

[35] S. Bowden, R. A. Sinton, *J. Appl. Phys.* **2007**, *102*, 12 124501.